

## Steady-State Magneto-Optical Trap with 100-Fold Improved Phase-Space Density

Shayne Bennetts, Chun-Chia Chen (陳俊嘉), Benjamin Pasquiou,\* and Florian Schreck  
*Van der Waals-Zeeman Institute, Institute of Physics, University of Amsterdam, Science Park 904,  
 1098XH Amsterdam, The Netherlands*

(Received 19 July 2017; published 1 December 2017)

We demonstrate a continuously loaded  $^{88}\text{Sr}$  magneto-optical trap (MOT) with a steady-state phase-space density of  $1.3(2) \times 10^{-3}$ . This is 2 orders of magnitude higher than reported in previous steady-state MOTs. Our approach is to flow atoms through a series of spatially separated laser cooling stages before capturing them in a MOT operated on the 7.4-kHz linewidth Sr intercombination line using a hybrid slower + MOT configuration. We also demonstrate producing a Bose-Einstein condensate at the MOT location, despite the presence of laser cooling light on resonance with the 30-MHz linewidth transition used to initially slow atoms in a separate chamber. Our steady-state high phase-space density MOT is an excellent starting point for a continuous atom laser and dead-time free atom interferometers or clocks.

DOI: 10.1103/PhysRevLett.119.223202

Laser cooled and trapped atoms are at the core of most ultracold quantum gas experiments [1], state-of-the-art clocks [2], and sensors based on atom interferometry [3]. Today, these devices typically operate in a time-sequential manner, with distinct phases for sample preparation and measurement. For atomic clocks a consequence is the need to bridge the dead time between measurements using a secondary frequency reference, typically a resonator. This introduces a problem known as the Dick effect [4], in which the sampling process inherent to a clock's cyclic operation down-converts or aliases high frequency noise from the secondary reference into the signal band, thus degrading performance [5]. Recently, a new generation of atomic clocks using degenerate atoms in a three-dimensional optical lattice has been demonstrated using Sr [6]. To reach the potential of such a clock, it will be necessary to overcome the Dick effect, which can be achieved by reducing the dead time and/or by creating vastly improved secondary references. Our steady-state MOT can lead to significant advances in both directions. It approaches the high flux and low temperature requirements needed for a steady-state clock, which would completely eliminate the Dick effect. Furthermore, our MOT is created under conditions compatible with the creation of degenerate samples or an atom laser [7,8]. This would be the ideal source for a secondary frequency reference based on superradiant lasing, which is expected to outperform current references [9–13]. Our source and a future atom laser based on it might also be valuable for atomic inertial sensors [8]. Improved clocks and inertial sensors will allow tests of fundamental physics [14] or be suitable for gravitational wave astronomy [3,15–17].

Over the years, many creative approaches have honed laser cooling to produce pulsed samples of ever increasing phase-space density (PSD) [18–29]. Pulsed MOTs using  $^{88}\text{Sr}$  have demonstrated phase-space densities of  $10^{-2}$  [30]

while atoms held in dipole traps recently reached degeneracy [7,31]. Despite the exquisite performances, these techniques suffer from extremely small capture velocities. As a consequence, atoms must first be captured and precooled, and thus these techniques have only been used as part of time-varying sequences.

Several continuous high PSD MOT schemes have been demonstrated mostly based on bichromatic MOTs using alkaline earth atoms [32,33]. The most successful reached a steady-state PSD of  $1.2 \times 10^{-5}$  [34]. This scheme used a MOT on a broad linewidth transition to capture atoms which then leak into a metastable state cooled by a MOT on a narrow transition. Narrow-line MOTs fed by a 2D MOT or Zeeman slower on the broad transition have been demonstrated for Yb and Er although steady-state PSDs are not measured [35,36]. Another approach is the dark SPOT MOT [37], which creates a central spatial region of reduced laser interaction. Adding a further steady-state trapping and cooling stage to a MOT can increase the PSD substantially [38–40], with a steady-state PSD of  $\sim 4 \times 10^{-4}$  reached for Cr atoms at a temperature of  $\sim 50 \mu\text{K}$  [40].

In this Letter, we demonstrate a  $^{88}\text{Sr}$  MOT at a temperature of  $\sim 2 \mu\text{K}$  and a steady-state phase-space density of  $1.3(2) \times 10^{-3}$ , 2 orders of magnitude higher than reported for previous steady-state MOTs [34]. Combining our MOT with techniques such as Refs. [7,38–42] promises yet higher PSDs and potentially a steady-state BEC and atom laser. Our result is achieved by flowing atoms through a series of spatially separated cooling stages as illustrated in Fig. 1. First we use the high capture velocity of the broad-linewidth, “blue,”  $^1S_0 - ^1P_1$  transition (30 MHz linewidth, 461 nm wavelength) in several stages to slow and cool atoms to mK temperatures, finishing with a 2D blue MOT. Next, we capture the atoms in a 3D MOT using the narrow-linewidth, “red,”  $^1S_0 - ^3P_1$  transition (7.4 kHz linewidth, 689 nm wavelength), which can reach temperatures close to

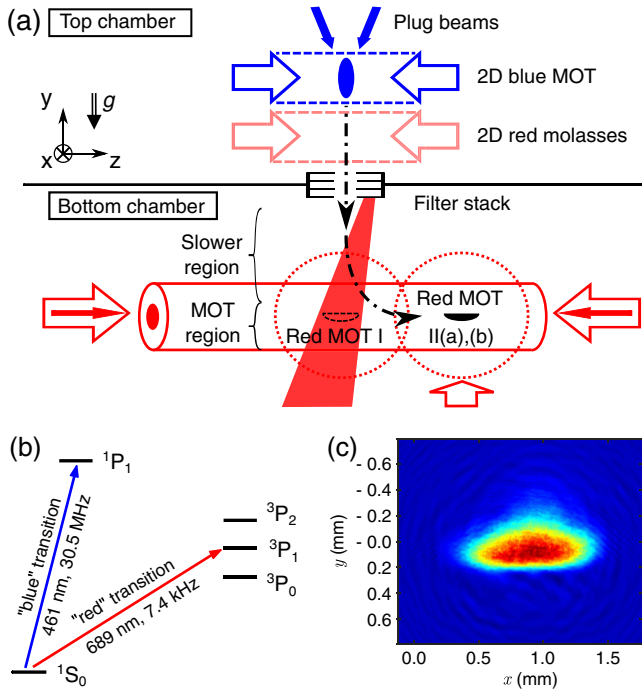


FIG. 1. (a) Schematic of our setup, showing the main cooling stages, and the position of the three red MOT configurations (see text). (b) Electronic level scheme of strontium, with the blue and red transitions used for laser cooling. (c) *In situ* absorption picture of a steady-state  $^{88}\text{Sr}$  MOT with a PSD of  $1.3(2) \times 10^{-3}$  [Red MOT II(b) configuration].

the recoil limit [30]. We operate the two MOTs in separate chambers to avoid heating of the 3D red MOT by blue photons scattered from surfaces and from fluorescing atoms in the 2D blue MOT. The transfer of atoms between chambers is ensured by two key ingredients: first, the atomic beam from the 2D blue MOT is collimated by a red optical molasses and second, the atoms are slowed in the second chamber by a hybrid slower + MOT configuration operated on the low capture velocity red transition. We show that this approach allows the red MOT to produce clouds with unprecedented phase-space densities for a steady-state apparatus. Furthermore, we show that the red MOT location is sufficiently protected to form BECs even with all the blue cooling stages operating.

The path of atoms through the setup begins with a high-flux atomic beam source adapted from our previous design [43–45]. In brief, this source is composed of an oven similar to Ref. [46], followed by a transverse cooling stage and a Zeeman slower, both using laser cooling on the broad-linewidth blue transition. A 2D blue MOT [47–49], whose nonconfining axis is oriented in the direction of gravity, is located approximately 5 cm after the exit of the Zeeman slower [see Fig. 1(a)]. This MOT has a loading rate of  $2.66(16) \times 10^9$   $^{88}\text{Sr}$  atoms/s (measured by absorption imaging) and cools atoms to about 1 mK in the radial ( $xz$ ) plane. To prevent atoms from escaping upward, a pair of

downward propagating blue “plug” beams are placed symmetrically to each other at an  $8^\circ$  angle from the  $y$  axis, increasing the flux by around 30%.

The high phase-space density MOT must be operated on the narrow-linewidth red transition while being protected against photons from the broad-linewidth blue transition [32]. In order to ensure such protection, we position the red MOT in a separate chamber, 41 cm below the 2D blue MOT. The two chambers are separated and baffled by a set of four stacked 1-inch absorptive neutral density filters (Thorlabs NE60A). These filters are separated by 20 mm and have an 8 mm diameter center hole allowing atoms to pass.

Upon exiting the 2D blue MOT, atoms have a radial velocity of about 0.5 m/s, an average downward velocity of 3 m/s [45], and they fall accelerated by gravity towards the bottom chamber. Radial expansion during the 185 mm drop to the bottom of the baffle section would give a transfer efficiency less than 2%. Accelerating the atoms downward is out of the question, since we can only use the low capture velocity red transition in the bottom chamber. Instead, we radially cool atoms emerging from the 2D MOT using a 2D molasses operating on the red  $^1S_0 - ^3P_1$   $\pi$  transition, which is insensitive to the spatially varying magnetic field. To compensate the Doppler broadening of the atomic transition, which is more than 100 times the 7.4 kHz natural linewidth, it is necessary to modulate the frequency of the molasses laser beams forming a frequency comb spanning from 30 to 750 kHz to the red of the transition, with 25 kHz spacing [44]. This technique is used on all our red-transition laser beams. To prevent the two red  $^1S_0 - ^3P_1$   $\sigma$  transitions towards the  $m_J = \pm 1$  states from hindering the radial slowing process, we produce a Zeeman shift of about 3 MHz by applying a bias magnetic field of 1.4 G in the vertical direction. Such a small field doesn’t disturb the operation of the 2D blue MOT. This molasses reaches steady state after a few 10 ms, easily provided by four horizontal molasses beams with  $1/e^2$  diameters of 45.6 mm along the  $y$  axis.

After a 41 cm fall from the top to the bottom chamber, the atomic beam has a measured downward velocity distribution peaked at 4 m/s. Our protection scheme necessitates slowing and capturing these falling atoms using only the red transition. However, the small scattering rate on this line allows a maximum deceleration of only  $\sim 16g$ , where  $g$  is earth acceleration. To overcome this extreme limitation we implement a hybrid slower + MOT.

Our first hybrid setup configuration labeled “Red MOT I” [see Fig. 1(a)] uses a magnetic quadrupole field centered 23 cm directly below the bottom baffle between chambers. The gradients are (0.55, 0.35, 0.23) G/cm in the ( $x, y, z$ ) directions. Horizontally propagating laser beams in the  $x, z$  axes are placed in a MOT configuration and provide radial cooling and confinement. On the  $y$  axis, a single, upward propagating beam is used, with circular polarization as needed for the MOT. Because of the weakness of the

transition this upward propagating beam and gravity are sufficient to confine atoms in the vertical direction without a downward propagating MOT beam [50]. The vertical beam is directed slightly to the side of the baffle onto the lowest neutral density filter, to prevent it from affecting the cooling processes in the top chamber. This beam is converging to exert a restoring force towards the beam center during the slowing process [51].

Upon reaching the second chamber, atoms enter the region illuminated by the circularly polarized upward-propagating beam, whose frequency is set to the red of the  $^1S_0 - ^3P_1$  transitions. We now describe the slowing process using an upward pointing quantization axis; see Fig. 2(a). The Doppler shift  $\delta_{\text{Doppler}}(v)$  of atoms with a downward velocity  $v$  brings them into resonance with the  $\sigma^+$  transition from  $^1S_0$  to the state  $m_J = +1$  of  $^3P_1$ . As radiation pressure slows atoms down,  $\delta_{\text{Doppler}}$  diminishes, which is partially compensated by the spatial variation of the magnetic field, following the principle of a Zeeman slower. The narrow linewidth of the red transition does not allow for a slowing process robust against magnetic and laser intensity fluctuations, so we modulate the laser frequency  $\nu_L$  with a span of  $\Delta\nu_L = 4.05$  MHz, as used for example in “white light” slowing [52]. If atoms are successfully slowed and reach the region below the quadrupole field center,  $\delta_{\text{Doppler}}$  is small and atoms are resonant with the laser light as in a standard broadband narrow-line MOT [30]. Note that for the experimental configurations used the angle between the local magnetic field and the beam direction can be big, leading to significant additional absorption on the  $\pi$  transition during the slowing process.

We numerically model this hybrid setup by evolving classical atomic trajectories, first in an idealized 1D geometry with only a linear vertical magnetic field gradient and a uniform circularly polarized vertical beam, and then using a Monte Carlo approach in a realistic 3D geometry including all beams and details of the magnetic fields [45]. The behavior of a falling atom can be obtained by analyzing the deceleration it experiences in dependence of time when dropped into the slower + MOT region with various starting velocities. The idealized 1D results shown in Fig. 2(b) are qualitatively confirmed by the more realistic 3D model results shown in Fig. 2(c). With these simulations we estimate a maximum capture velocity of around 6 m/s for the hybrid slower + MOT setup, which is compatible with the measured velocity distribution of the atomic beam produced by the 2D blue MOT [45].

The characteristics of the hybrid Red MOT I are summarized in Table I. The loading rate gives an estimated transfer efficiency of 19% between the two chambers. Unfortunately, the high power broadband beams needed for the hybrid setup limit the PSD to  $2.8(1.2) \times 10^{-6}$ , low compared to what can be achieved with a pure red MOT geometry in a time-varying sequence [30]. Moreover, with direct line-of-sight to a bright fluorescing blue MOT, this configuration does not provide protection against heating

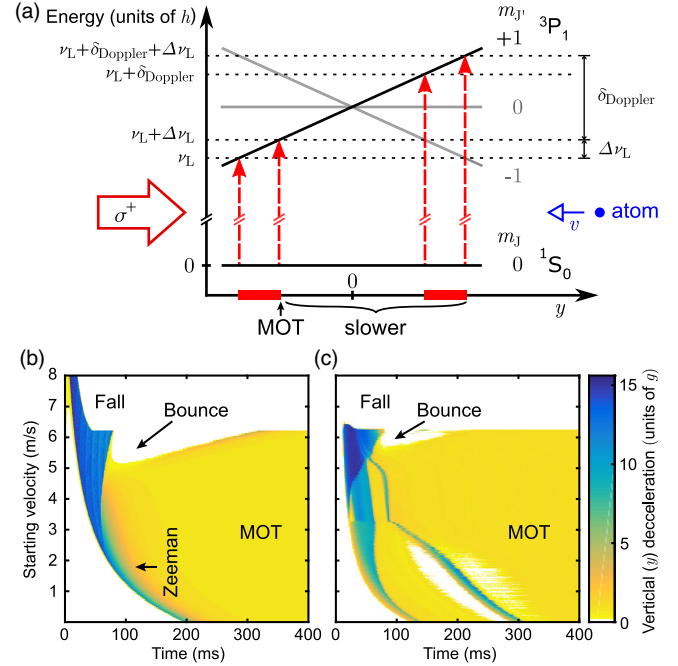


FIG. 2. Working principle of the hybrid slower + MOT in Red MOT I configuration. (a) Energy diagram of the  $^1S_0$ ,  $m_J$ , and the  $^3P_1$ ,  $m_J$  states in dependence of  $y$  for  $x = z = 0$ , where the coordinate origin lays in the quadrupole field center. An atom with velocity  $v \neq 0$  along the  $y$  axis is addressed by the upward-propagating Red MOT I beam in a region delimited by the pair of red dashed arrows on the right. The range of this region is determined by the span of the laser frequency modulation  $\Delta\nu_L$  and the magnetic field gradient. An atom with  $v = 0$  is addressed in the region delimited by the pair of dashed arrows on the left. (b)  $y$  deceleration from scattering of photons on the red transition (in units of earth acceleration  $g$ ) in dependence of the initial velocity of atoms 20 cm above the quadrupole field center, obtained by an idealized 1D calculation. A horizontal path across the diagram corresponds to a 1D time-dependent trajectory along  $y$ . Annotations indicate regions dominated by Zeeman type slowing or red MOT type trapping. Atoms eventually captured in the MOT exhibit a time-independent non-zero force (yellow region at  $\sim 1g$ ). The white regions show decelerations smaller than  $0.25g$ . The “Bounce” and “Fall” regions are undesirable cases described in Ref. [45]. (c) Equivalent deceleration data obtained by a full 3D Monte Carlo calculation with a realistic geometry.

from blue photons sufficient to produce a steady-state BEC [45].

For these reasons, we implement a second MOT configuration, “Red MOT II(a),” located 3 cm in the  $z$  direction away from the Red MOT I position [see Fig. 1(a)]. This is achieved by adding another 5-beam geometry MOT (4 beams along  $x$  and  $z$ , 1 beam along  $y$ ), whose beams make a smooth connection with the Red MOT I beams, and by displacing the center of the quadrupole field to the intersection of these new beams. Along the  $z$  axis the two additional beams are implemented as an 8 mm diameter low-intensity core within hollow 48 mm diameter Red

TABLE I. Characteristics of the three Red MOT configurations. All uncertainties stated in this letter are taken as  $\pm 2\sigma$  from the fitted data.

	Red MOT I	Red MOT II(a)	Red MOT II(b)
Flux [ $^{88}\text{Sr}/\text{s}$ ]	$5.1(7) \times 10^8$	$5.3(4) \times 10^7$	$5.3(9) \times 10^6$
Temperature $x$	... <sup>a</sup>	$3.7(3) \mu\text{K}$	$2.01(6) \mu\text{K}$
Temperature $y$	$20(5) \mu\text{K}$	$1.9(1) \mu\text{K}$	$1.42(3) \mu\text{K}$
Temperature $z$	$26(7) \mu\text{K}$	$2.8(2) \mu\text{K}$	$1.91(9) \mu\text{K}$
Width $\sigma_x$	... <sup>a</sup>	$385(4) \mu\text{m}$	$150(2) \mu\text{m}$
Width $\sigma_y$	$725(61) \mu\text{m}$	$192(3) \mu\text{m}$	$88(1) \mu\text{m}$
Width $\sigma_z$	$2086(41) \mu\text{m}$	$528(3) \mu\text{m}$	$247(3) \mu\text{m}$
Atom number [ $^{88}\text{Sr}$ ]	$2.54(10) \times 10^9$	$1.71(5) \times 10^8$	$2.5(1) \times 10^7$
Peak density [ $^{88}\text{Sr}/\text{cm}^3$ ]	$5.1(7) \times 10^{10}$	$2.8(2) \times 10^{11}$	$4.8(4) \times 10^{11}$
Peak PSD	$2.8(1.2) \times 10^{-6}$	$4(1) \times 10^{-4}$	$1.3(2) \times 10^{-3}$
$1/e$ lifetime	$4.53(6) \text{ s}$	$2.8(2) \text{ s}$	$1.95(6) \text{ s}$

<sup>a</sup>At the location of Red MOT I no imaging system for the  $x$  axis was available so Red MOT I density and PSD calculations assume that temperature and width are the same as  $z$  along  $x$ .

MOT I beams. In this configuration, atoms entering the second chamber are decelerated by the hybrid slower plus Red MOT I beams, then continuously pushed to the Red MOT II(a) where they are confined and further cooled. The working principle of the hybrid setup remains unchanged, with the exception that the  $\pi$  transition becomes more important, since the magnetic field lines are more tilted with respect to the Red MOT I vertical beam.

Within this second red MOT, we have more freedom to adapt the beam parameters and thereby reach higher PSD. The main limitations to the PSD are first power broadening of the red transition effectively raising the Doppler cooling limit, and second multiple scattering due to the high density. Both limitations recede with reduced MOT powers. For this reason, we implement a spectrally dark SPOT MOT by shaping the spectral intensity profile of our broadband MOT beams. At the steady-state MOT location, the effective scattering rate is just enough to hold atoms against gravity, while in the surrounding region an effective high optical power captures fast atoms.

With Red MOT II(a) using the parameters given in Table I, we reach a steady-state MOT with a PSD of  $4(1) \times 10^{-4}$  for  $^{88}\text{Sr}$ . The transfer efficiency from the top chamber to this MOT is 2%, an order of magnitude lower than for Red MOT I. Simulations suggest significant losses may be attributed first to increased bouncing of atoms in the hybrid slower when the  $\pi$  transition is dominant, and second to atom trajectories intersecting with mirrors inside the vacuum chamber.

We also produce a Red MOT II(a) using the much less abundant  $^{84}\text{Sr}$  isotope, which is particularly suited to produce quantum degenerate gases, owing to its favorable scattering properties. This  $^{84}\text{Sr}$  MOT contains up to  $9.0(2) \times 10^6$  atoms at temperatures of  $1.5(3) \mu\text{K}$  and  $3.4(1.1) \mu\text{K}$  in the vertical and horizontal axes, respectively. By loading this MOT into an optical dipole trap in a time sequential manner and applying a 3 s evaporative cooling sequence, we produce  $^{84}\text{Sr}$  BECs of  $3.0(2) \times 10^5$  atoms.

The protection provided by the dual chamber and baffle system against photons from the broad-linewidth blue transition is determined by comparing the BEC lifetime at the location of the Red MOT II(a) with and without the 2D blue MOT operating. The atomic flux is disabled by turning off the red transition beams during these measurements. The BEC lifetime in the dipole trap is  $3.0(4) \text{ s}$  without blue light and  $2.7(2) \text{ s}$  with blue light. Lifetimes were strongly limited by one-body collisions due to poor vacuum quality. These measurements confirm significant protection from blue photons thanks to our two-chamber design, making our system suitable for experiments aimed at developing a steady-state source of degenerate quantum gas.

Finally, “Red MOT II(b)” is a configuration designed to optimize phase-space density at the expense of transfer efficiency. This MOT reaches a steady-state PSD of  $1.3(2) \times 10^{-3}$  for  $^{88}\text{Sr}$ , which is 2 orders of magnitude higher than demonstrated in previous steady-state MOTs [34] [see Fig. 1(c) and Table I]. Red MOT II(b) is the same as Red MOT II(a) except that we reduce the bandwidth of the MOT II beams to cover only  $-40$  to  $-200 \text{ kHz}$  detuning, resulting in three improvements. First, the smaller detuning of  $-40 \text{ kHz}$  compresses the MOT, second, the reduced bandwidth reduces the total beam intensity required, and third, by ending the spectrum well before the photoassociation line located at  $-435 \text{ kHz}$  detuning [53], we reduce losses due to molecule formation. The transfer efficiency from the top chamber to this MOT is 0.2%, an order of magnitude lower than for Red MOT II(a). The  $1/e$  lifetime of Red MOT II(b) measured after the atomic flux is suddenly stopped is  $1.95(6) \text{ s}$ , which is significantly smaller than the  $4.53(6) \text{ s}$  lifetime of Red MOT I. This reduction is due to two-body light-assisted collisions, which ultimately limits the maximum density achievable [53]. Both these losses and the need to compensate for gravity set the limits on the PSD achievable with this MOT configuration.

To summarize, we have demonstrated the operation of a MOT with a PSD of  $1.3(2) \times 10^{-3}$  in the steady-state regime. This result requires the use of broad- and narrow-linewidth transitions to simultaneously achieve both high PSD and high capture efficiency. We use a dual chamber architecture to protect the MOT from heating by broad-linewidth transition photons, and efficient transfer between chambers is achieved using a hybrid slower + MOT configuration using only cooling on the narrow-linewidth transition. Although Sr is ideally suited to this architecture, our approach is broadly applicable to alkaline-earth metals, lanthanides, and any other species with a strong transition to precool atoms and a weak transition supporting the operation of a MOT with a high PSD [54,55]. Finally, we have shown that our design is compatible with the generation of quantum degenerate gases in the presence of a laser cooled influx. The use of this high-PSD source of matter, combined with a protection mechanism such as that demonstrated in Ref. [7], should allow the creation of a steady-state Bose-Einstein condensate and ultimately an atom laser with uninterrupted phase coherent output.

We thank Georgios Siviloglou for contributions during the early stages of the design and construction of the experiment. We thank the Netherlands Organisation for Scientific Research (NWO) for funding through Vici grant No. 680-47-619. This project has received funding from the European Research Council (ERC) under the European Union's Seventh Framework Programme (FP7/2007-2013) (Grant agreement No. 615117 QuantStro). B. P. thanks the NWO for funding through Veni Grant No. 680-47-438 and C.-C. C. thanks the Ministry of Education of the Republic of China (Taiwan) for a MOE Technologies Incubation Scholarship. S. B. thanks the Australian Government and Nick Robins at the Australian National University for an Australian Postgraduate Award and support during the early stages of this work.

S. B. and C.-C. C. contributed equally to this work.

\*highPSDMOT@strontiumBEC.com

- [1] I. Bloch, J. Dalibard, and W. Zwerger, Many-body physics with ultracold gases, *Rev. Mod. Phys.* **80**, 885 (2008).
- [2] A. D. Ludlow, M. M. Boyd, J. Ye, E. Peik, and P. O. Schmidt, Optical atomic clocks, *Rev. Mod. Phys.* **87**, 637 (2015).
- [3] A. D. Cronin, J. Schmiedmayer, and D. E. Pritchard, Optics and interferometry with atoms and molecules, *Rev. Mod. Phys.* **81**, 1051 (2009).
- [4] G. J. Dick, Local oscillator induced instabilities in trapped ion frequency standards, in *Proceedings of the Precise Time and Time Interval Meeting*, edited by R. Sydnor (U.S. Naval Observatory, Washington, DC, 1987), p. 133.
- [5] P. G. Westergaard, J. Lodewyck, and P. Lemonde, Minimizing the dick effect in an optical lattice clock, *IEEE Trans. Ultrason. Ferroelectr. Freq. Control* **57**, 623 (2010).
- [6] S. L. Campbell, R. B. Hutson, G. E. Marti, A. Goban, N. D. O'Connell, R. L. McNally, L. Sonderhouse, J. M. Robinson, W. Zhang, B. J. Bloom, and J. Ye, A Fermi-degenerate three-dimensional optical lattice clock, *Science* **358**, 90 (2017).
- [7] S. Stellmer, B. Pasquiou, R. Grimm, and F. Schreck, Laser Cooling to Quantum Degeneracy, *Phys. Rev. Lett.* **110**, 263003 (2013).
- [8] N. P. Robins, P. A. Altin, J. E. Debs, and J. D. Close, Atom lasers: Production, properties and prospects for precision inertial measurement, *Phys. Rep.* **529**, 265 (2013).
- [9] J. Chen, Active optical clock, *Chin. Sci. Bull.* **54**, 348 (2009).
- [10] D. Meiser, J. Ye, D. R. Carlson, and M. J. Holland, Prospects for a Millihertz-Linewidth Laser, *Phys. Rev. Lett.* **102**, 163601 (2009).
- [11] D. Meiser and M. J. Holland, Steady-state superradiance with alkaline-earth-metal atoms, *Phys. Rev. A* **81**, 033847 (2010).
- [12] D. G. Matei, T. Legero, S. Häfner, C. Grebing, R. Weyrich, W. Zhang, L. Sonderhouse, J. M. Robinson, J. Ye, F. Riehle, and U. Sterr, 1.5  $\mu\text{m}$  Lasers with Sub-10 mHz Linewidth, *Phys. Rev. Lett.* **118**, 263202 (2017).
- [13] M. A. Norcia, M. N. Winchester, J. R. K. Cline, and J. K. Thompson, Superradiance on the millihertz linewidth strontium clock transition, *Sci. Adv.* **2**, e1601231 (2016).
- [14] J.-P. Uzan, The fundamental constants and their variation: observational and theoretical status, *Rev. Mod. Phys.* **75**, 403 (2003).
- [15] P. W. Graham, J. M. Hogan, M. A. Kasevich, and S. Rajendran, New Method for Gravitational Wave Detection with Atomic Sensors, *Phys. Rev. Lett.* **110**, 171102 (2013).
- [16] N. Yu and M. Tinto, Gravitational wave detection with single-laser atom interferometers, *Gen. Relativ. Gravit.* **43**, 1943 (2011).
- [17] S. Kolkowitz, I. Pikovski, N. Langellier, M. D. Lukin, R. L. Walsworth, and J. Ye, Gravitational wave detection with optical lattice atomic clocks, *Phys. Rev. D* **94**, 124043 (2016).
- [18] P. D. Lett, R. N. Watts, C. I. Westbrook, W. D. Phillips, P. L. Gould, and H. J. Metcalf, Observation of Atoms Laser Cooled below the Doppler Limit, *Phys. Rev. Lett.* **61**, 169 (1988).
- [19] J. Dalibard and C. Cohen-Tannoudji, Laser cooling below the Doppler limit by polarization gradients: simple theoretical models, *J. Opt. Soc. Am. B* **6**, 2023 (1989).
- [20] G. Salomon, L. Fouche, P. Wang, A. Aspect, P. Bouyer, and T. Bourdel, Gray-molasses cooling of  $^{39}\text{K}$  to a high phase-space density, *Europhys. Lett.* **104**, 63002 (2013).
- [21] G. Colzi, G. Durastante, E. Fava, S. Serafini, G. L'Amorese, and G. Ferrari, Sub-Doppler cooling of sodium atoms in gray molasses, *Phys. Rev. A* **93**, 023421 (2016).
- [22] M. Kasevich and S. Chu, Laser Cooling Below a Photon Recoil with Three-Level Atoms, *Phys. Rev. Lett.* **69**, 1741 (1992).
- [23] A. Aspect, E. Arimondo, R. Kaiser, N. Vansteenkiste, and C. Cohen-Tannoudji, Laser Cooling below the One-Photon Recoil Energy by Velocity-Selective Coherent Population Trapping, *Phys. Rev. Lett.* **61**, 826 (1988).

- [24] J. Rühlig, T. Bäuerle, A. Griesmaier, and T. Pfau, High efficiency demagnetization cooling by suppression of light-assisted collisions, *Opt. Express* **23**, 5596 (2015).
- [25] S. E. Hamann, D. L. Haycock, G. Klose, P. H. Pax, I. H. Deutsch, and P. S. Jessen, Resolved-Sideband Raman Cooling to the Ground State of an Optical Lattice, *Phys. Rev. Lett.* **80**, 4149 (1998).
- [26] A. J. Kerman, V. Vuletić, C. Chin, and S. Chu, Beyond Optical Molasses: 3D Raman Sideband Cooling of Atomic Cesium to High Phase-Space Density, *Phys. Rev. Lett.* **84**, 439 (2000).
- [27] D.-J. Han, S. Wolf, S. Oliver, C. McCormick, M. T. DePue, and D. S. Weiss, 3D Raman Sideband Cooling of Cesium Atoms at High Density, *Phys. Rev. Lett.* **85**, 724 (2000).
- [28] C. Y. Yang, P. Halder, O. Appel, D. Hansen, and A. Hemmerich, Continuous loading of  $^1S_0$  calcium atoms into an optical dipole trap, *Phys. Rev. A* **76**, 033418 (2007).
- [29] N. Radwell, G. Walker, and S. Franke-Arnold, Cold-atom densities of more than  $10^{12} \text{ cm}^{-3}$  in a holographically shaped dark spontaneous-force optical trap, *Phys. Rev. A* **88**, 043409 (2013).
- [30] H. Katori, T. Ido, Y. Isoya, and M. Kuwata-Gonokami, Magneto-Optical Trapping and Cooling of Strontium Atoms down to the Photon Recoil Temperature, *Phys. Rev. Lett.* **82**, 1116 (1999).
- [31] J. Hu, A. Urvoy, Z. Vendeiro, V. Crépel, W. Chen, and V. Vuletić, Creation of a Bose-condensed gas of  $^{87}\text{Rb}$  by laser cooling, *Science* **358**, 1078 (2017).
- [32] A. Kawasaki, B. Braverman, Q. Yu, and V. Vuletić, Two-color magneto-optical trap with small magnetic field for ytterbium, *J. Phys. B* **48**, 155302 (2015).
- [33] J. Lee, J. H. Lee, J. Noh, and J. Mun, Core-shell magneto-optical trap for alkaline-earth-metal-like atoms, *Phys. Rev. A* **91**, 053405 (2015).
- [34] J. Grünert and A. Hemmerich, Sub-Doppler magneto-optical trap for calcium, *Phys. Rev. A* **65**, 041401 (2002).
- [35] S. Dörscher, A. Thobe, B. Hundt, A. Kochanke, R. L. Targat, P. Windpassinger, C. Becker, and K. Sengstock, Creation of quantum-degenerate gases of ytterbium in a compact 2D-/3D-magneto-optical trap setup, *Rev. Sci. Instrum.* **84**, 043109 (2013).
- [36] A. Frisch, K. Aikawa, M. Mark, A. Rietzler, J. Schindler, E. Zupanič, R. Grimm, and F. Ferlaino, Narrow-line magneto-optical trap for erbium, *Phys. Rev. A* **85**, 051401 (2012).
- [37] W. Ketterle, K. B. Davis, M. A. Joffe, A. Martin, and D. E. Pritchard, High Densities of Cold Atoms in a Dark Spontaneous-Force Optical Trap, *Phys. Rev. Lett.* **70**, 2253 (1993).
- [38] J. Mahnke, I. Kruse, A. Hüper, S. Jöllenbeck, W. Ertmer, J. Arlt, and C. Klempt, A continuously pumped reservoir of ultracold atoms, *J. Phys. B* **48**, 165301 (2015).
- [39] M. Falkenau, V. V. Volchkov, J. Rühlig, A. Griesmaier, and T. Pfau, Continuous Loading of a Conservative Potential Trap from an Atomic Beam, *Phys. Rev. Lett.* **106**, 163002 (2011).
- [40] V. V. Volchkov, J. Rühlig, T. Pfau, and A. Griesmaier, Sisyphus cooling in a continuously loaded trap, *New J. Phys.* **15**, 093012 (2013).
- [41] A. P. Chikkatur, Y. Shin, A. E. Leanhardt, D. Kielpinski, E. Tsikata, T. L. Gustavson, D. E. Pritchard, and W. Ketterle, A continuous source of Bose-Einstein condensed atoms, *Science* **296**, 2193 (2002).
- [42] N. P. Robins, C. Figl, M. Jeppesen, G. R. Dennis, and J. D. Close, A pumped atom laser, *Nat. Phys.* **4**, 731 (2008).
- [43] S. Stellmer, Ph.D. thesis, University of Innsbruck, 2013.
- [44] S. Stellmer, M. K. Tey, B. Huang, R. Grimm, and F. Schreck, Bose-Einstein Condensation of Strontium, *Phys. Rev. Lett.* **103**, 200401 (2009).
- [45] See Supplemental Material at <http://link.aps.org/supplemental/10.1103/PhysRevLett.119.223202> for in-depth information about our apparatus and approach.
- [46] R. Senaratne, S. V. Rajagopal, Z. A. Geiger, K. M. Fujiwara, V. Lebedev, and D. M. Weld, Effusive atomic oven nozzle design using an aligned microcapillary array, *Rev. Sci. Instrum.* **86**, 023105 (2015).
- [47] K. Dieckmann, R. J. C. Spreeuw, M. Weidemüller, and J. T. M. Walraven, Two-dimensional magneto-optical trap as a source of slow atoms, *Phys. Rev. A* **58**, 3891 (1998).
- [48] T. Yang, K. Pandey, M. S. Pramod, F. Leroux, C. C. Kwong, E. Hagiyeve, Z. Y. Chia, B. Fang, and D. Wilkowski, A high flux source of cold strontium atoms, *Eur. Phys. J. D* **69**, 226 (2015).
- [49] I. Nosske, L. Couturier, F. Hu, C. Tan, C. Qiao, J. Blume, Y. H. Jiang, P. Chen, and M. Weidemüller, Two-dimensional magneto-optical trap as a source for cold strontium atoms, *Phys. Rev. A* **96**, 053415 (2017).
- [50] M. K. Tey, S. Stellmer, R. Grimm, and F. Schreck, Double-degenerate Bose-Fermi mixture of strontium, *Phys. Rev. A* **82**, 011608 (2010).
- [51] J. V. Prodan, W. D. Phillips, and H. Metcalf, Laser Production of a Very Slow Monoenergetic Atomic Beam, *Phys. Rev. Lett.* **49**, 1149 (1982).
- [52] M. Zhu, C. W. Oates, and J. L. Hall, Continuous High-Flux Monovelocity Atomic Beam Based on a Broadband Laser-Cooling Technique, *Phys. Rev. Lett.* **67**, 46 (1991).
- [53] M. Borkowski, P. Morzyński, R. Ciuryło, P. S. Julienne, M. Yan, B. J. DeSalvo, and T. C. Killian, Mass scaling and nonadiabatic effects in photoassociation spectroscopy of ultracold strontium atoms, *Phys. Rev. A* **90**, 032713 (2014).
- [54] A. J. Berglund, J. L. Hanssen, and J. J. McClelland, Narrow-Line Magneto-Optical Cooling and Trapping of Strongly Magnetic Atoms, *Phys. Rev. Lett.* **100**, 113002 (2008).
- [55] T. Kuwamoto, K. Honda, Y. Takahashi, and T. Yabuzaki, Magneto-optical trapping of Yb atoms using an intercombination transition, *Phys. Rev. A* **60**, R745 (1999).